June 1990

# Control of Vortical Separation on a Circular Cone

Nikos J. Mourtos
*San Jose State University*, Nikos.Mourtos@sjsu.edu

# Control of vortical separation on a circular cone

**N. J. MOURTOS**
Department of Aerospace Engineering, San Jose State University, California, USA

## ABSTRACT

For conical bodies, at moderate angles of attack, the flow separates from the lee side, forming two vortices. Although the vortex lift contribution is highly desirable, as the angle of attack increases, the vortex system becomes asymmetric, and eventually the vortices breakdown. Thus, some control of the separation process is necessary if the vortex lift is to be exploited at higher angles of attack.

The theoretical model which is used in this analysis has three parts. First, the 'single line-vortex' model is used within the framework of 'slender-body theory' to compute the outer inviscid field for specified separation lines. Second, the 3-D boundary layer is represented by a momentum equation for the cross-flow, analogous to that for a plane boundary layer and a von Karman/Pohlhausen approximation is applied to solve this equation. The cross-flow separation for both laminar and turbulent layers is determined by matching the pressure at the upper and lower separation points. This iterative procedure yields a unique solution for the separation lines and consequently for the positions of the vortices and the vortex lift on the body. Third, control of separation is achieved by blowing tangentially from slots located symmetrically along cone generators.

## NOMENCLATURE

| | |
|---|---|
| $b_j$ | jet half width |
| $C_p$ | pressure coefficient |
| $C\mu$ | blowing coefficient |
| $p$ | static pressure |
| $R$ | local radius of the cone |
| $u$, $v$, $w$ | velocities in $\xi$, $\eta$ and $\zeta$ directions |
| $V$ | dimensionless velocity in $\eta$ direction |
| $\alpha$ | angle of attack |
| $\delta$ | boundary layer thickness |
| $\delta_1$, $\delta_2$ | displacement thickness in $\xi$ and $\eta$ directions respectively |
| $\epsilon$ | cone semi-apex angle |
| $\theta$ | angular coordinate, momentum thickness |
| $\theta_{21}$ | momentum thickness due to the mutual effect of the longitudinal and circumferential flows |
| $\theta_{22}$ | momentum thickness in $\eta$ direction |
| $\nu$ | kinematic viscosity |
| $\xi$, $\eta$, $\zeta$ | conical coordinates in the direction of a generator, circumference of the cross section and normal to the surface respectively |
| $\rho$ | fluid density |
| $\tau$ | wall shear stress |

### Subscripts

| | |
|---|---|
| $e$ | inviscid external flow |
| $m$ | maximum velocity point in the jet |
| $rp$ | reattachment point |
| $s$ | separation point |
| $su$ | upper separation point |
| $sl$ | lower separation point |
| $st$ | windward stagnation point |

Manuscript received 21 September 1989, revised version received 12 March 1990, accepted 19 March 1990.
Paper No 1752.

## INTRODUCTION

In a variety of aeronautical as well as aerospace applications, the flow around conical bodies at high angle of attack is of interest. For such conical bodies, even at small to moderate angles of attack, the flow separates from the lee side, forming a pair of vortices. The contribution of vortex lift at low angles of attack is highly desirable. As the angle of attack increases, and the vortex system becomes first asymmetric, then unstable and uncontrollable, a large dependance on vortex lift may cause serious problems with longitudinal and lateral stability. Therefore, if the formation of the vortices could be controlled, vehicle operation could be extended to higher angles of attack.

The motivation for the present analytical study was provided by the experimental work of Wood and Roberts[1]. They found that it is possible to control the cross-flow boundary layer separation and hence affect the outer flow field of a conical delta wing by blowing tangentially from slots located symmetrically along cone generators.

The purpose of the present work is three-fold:

First, to explore the influence of the position of separation on the vortex parameters (location, strength, lift). This is done through an inviscid analysis of the outer field, for arbitrarily chosen separation lines.

Second, to uniquely determine the separation line locations through a boundary layer (viscous) analysis.

Third, to analyse the control of boundary layer separation by wall jet blowing. This also requires a viscous analysis and is based on the idea that a thin high-velocity layer of fluid ejected tangentially to the surface of the body reenergises the boundary layer and makes it less susceptible to separation.

For more details on the present work the reader should refer to Ref. 2. Here only the important results are presented.

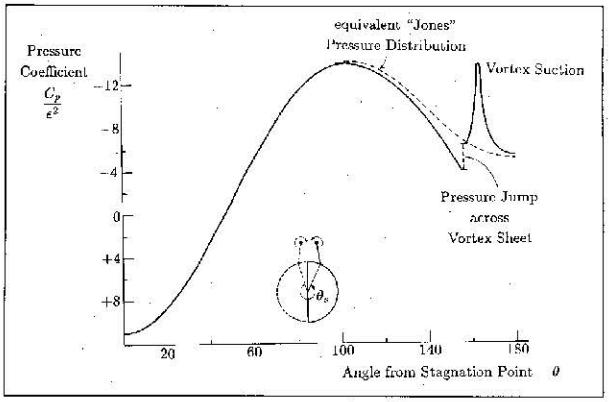


Figure 1. Pressure distribution on a circular cone for $\theta_s = 157°$ and $\alpha/\epsilon = 2$.

## INVISCID ANALYSIS

The 'single line-vortex' model (SLV) is the simplest way to represent the leeside separation on conical bodies. Although it lacks accuracy, it was chosen over more realistic models because of its simplicity. Simplicity is an important feature when it is necessary to iterate the inviscid solution with a viscous one in order to determine the actual separation lines.

The flow separation is represented by a pair of line vortices which are fed with vorticity through a pair of planar vortex sheets emanating from the inviscid separation lines on the body surface. Although the 2-D Laplace equation governs the velocity potential, the three-dimensionality of the problem enters through the boundary condition which requires that the vortex system (line-vortex and planar vortex sheet) is force-free.

The SLV model has been applied to a circular cone by Byrson[3] for separation lines located symmetrically at $\theta_s = 147°$ (where $\theta$ is the angle measured from the windward generator). In the present analysis, the location of separation is varied, and the effect of this variation on the vortex parameters (position, strength, lift) is studied. The results from the inviscid analysis[2] may be summarised as follows:

The vortices move closer to the surface of the cone and become weaker as the separation lines shift toward the leeward generator.

The lift on a circular cone at incidence has two components, the Jones lift and the vortex lift. The Jones lift is calculated assuming attached flow everywhere on the body's surface and grows linearly with angle of attack[4]. The vortex lift grows non-linearly with angle of attack.

As the primary separation lines are moved toward the leeward generator, vortex lift is suppressed and in the limit, as the separation lines coincide with the leeward generator, the Jones solution is recovered.

This suggests that displacing the primary separation is indeed a viable mechanism for controlling vortex position and vortex lift, a fact that has already been verified experimentally[1].

The pressure distribution on a circular cone with leeside separation is shown in Fig. 1 together with the pressure distribution for totally attached flow. There are three features which differentiate the pressure distribution for separated flow from that of attached flow:

the presence of vortex suction
the pressure jump across the vortex sheet
the presence of two adverse pressure gradients (versus only one for the attached flow).

## CONICAL BOUNDARY LAYER ANALYSIS

For the inviscid analysis, the separation lines were placed arbitrarily; in reality, the position of separation must be determined through a viscous analysis. The velocity and pressure fields computed for the outer inviscid field are used as boundary conditions for the boundary layer equations; integration of these equations yields two locations where the boundary layer leaves the surface, one on each side of the hypothetical separation line.

The boundary layer equations for a slender cone are as follows:

continuity

$$u + \xi \frac{\partial u}{\partial \zeta} + \frac{1}{\varepsilon}\frac{\partial v}{\partial \eta} + \xi \frac{\partial w}{\partial \zeta} = 0 \qquad . \; . \; . \quad (1)$$

momentum in $\xi$-direction

$$u\frac{\partial u}{\partial \xi} + \frac{v}{\varepsilon\xi}\frac{\partial u}{\partial \eta} + w\frac{\partial u}{\partial \zeta} - \frac{v^2}{\xi} = \frac{1}{\rho}\frac{\partial \tau_\xi}{\partial \zeta} \qquad . \; . \; . \quad (2)$$

momentum in $\eta$-direction

$$u\frac{\partial v}{\partial \xi} + \frac{v}{\varepsilon\xi}\frac{\partial v}{\partial \eta} + w\frac{\partial v}{\partial \zeta} + \frac{uv}{\xi} = -\frac{1}{\rho\varepsilon\xi}\frac{\partial p}{\partial \eta} + \frac{1}{\rho}\frac{\partial \tau_\eta}{\partial \zeta}$$

$$. \; . \; . \quad (3)$$

momentum in $\zeta$-direction

$$\frac{\partial p}{\partial \zeta} = 0 \qquad . \; . \; . \quad (4)$$

while for conical external flow we also have

$$\frac{\partial u_e}{\partial \eta} = \varepsilon v_e \qquad . \; . \; . \quad (5)$$

$$-\frac{1}{\rho}\frac{\partial p}{\partial \eta} = v_e\left(\frac{\partial v_e}{\partial \eta} + \varepsilon u_e\right) \qquad . \; . \; . \quad (6)$$

Next, equation (3) is integrated across the boundary layer (i.e., from $\zeta = 0$ at the surface of the cone to $\zeta \to \infty$ outside the boundary layer), while the normal velocity component $w$ is substituted from equation (1). Using appropriate displacement and momentum thicknesses as described in the nomenclature, the integral form of the cross-flow boundary layer equation can be written as

$$v_e^2\frac{\partial \theta_{22}}{\partial \eta} + \left(v_e\frac{\partial v_e}{\partial \eta} + \varepsilon u_e v_e\right)(\delta_2 + 2\theta_{22})$$

$$+ \varepsilon u_e v_e[\delta_1 - \delta_2 + (n+2)\theta_{21} - 2\theta_{22}] = \frac{\tau_n R}{\rho}$$

$$. \; . \; . \quad (7)$$

Here $n$ is the exponent in the boundary layer growth expression

$$\delta = k\xi^n \qquad \ldots \quad (8)$$

where $k$ is a constant.

Equation (7) is similar to the corresponding momentum equation for a 2-D boundary layer, the primary difference being the presence of the last term on the left side which contains the momentum thicknesses due to the interaction of the longitudinal and circumferential flows.

No assumptions were made regarding the state of the boundary layer. Therefore, equation (7) is valid for both laminar and turbulent boundary layers, on condition that in the latter case $u$ and $v$ denote the time average of the respective velocity components. The primary difference between the two cases (i.e. laminar and turbulent) will be the rate of growth of the boundary layer in equation (8). In the laminar case $n = 0{\cdot}5$ while in the turbulent case $n = 0{\cdot}8$.

The last term on the left-hand side of equation (7) was evaluated numerically for several cases ($\alpha$,$\varepsilon$) and several locations ($\eta$) along the boundary layer. Its maximum contribution to the total value of the shear stress on the right-hand side was approximately 13% for the laminar layer and 21% for the turbulent layer. At separation, its contribution was only 0·6% and 0·9% respectively for the two cases. Thus, it seems reasonable to neglect this term. When this is done, equation (7) becomes exactly analogous to the corresponding equation for the 2-D boundary layer. The solution is found by the Karman/Pohlhausen method[5]. Table 1 illustrates the analogy between the various quantities involved in the 2-D and conical boundary layers.

**TABLE 1**
**Analogy between 2-D and conical (laminar) boundary layers**

| 2-D ($x$, $y$) | Conical ($\xi$, $\eta$, $\zeta$) |
|---|---|
| momentum equation<br>$\tau/\rho = v_e^2\,(d\theta_1/dx) +$<br>$(\delta_1 + 2\theta_1)v_e(dv_e/dx)$ | $\tau/\rho = v_e^2\,(\partial\theta_{22}/\partial\eta) +$<br>$v_e(\delta_2 + 2\theta_{22})[(\partial v_e/\partial\eta) + (\varepsilon u_e/R)]$ |
| first shape factor<br>$\Lambda = (\delta^2/\nu)(dv_e/dx$ | $\Lambda = (\delta^2/\nu)[(\partial v_e/\partial\eta + (\varepsilon u_e/R)]$ |
| second shape factor<br>$K = (\theta_1^2/\delta^2)\Lambda$ | $K = (\theta_{22}^2/\delta^2)\Lambda$ |
| third shape factor<br>$H = (\delta_1/\theta_1)$ | $H = (\delta_2/\theta_{22})$ |
| solution<br>$\theta_1^2 = 0{\cdot}47\nu/Ev_e^6)\int_0^x Ev_e^5 dx$ | $\theta_{22}^2 = 0{\cdot}47\nu/Ev_e^6)\int_0^\eta Ev_e^5 d\eta$ |
| $E = 1$ | $E = \exp\{6\varepsilon\int_0^\eta (u_e/v_e)d\eta\}$ |

The separation criteria are also taken directly from the 2-D case (Table 2). These criteria can be expressed as integral functions of the velocity outside the boundary layer.

The matching of the viscous and inviscid flow fields is illustrated in Fig. 2. For a specified separation angle $\theta_s$, velocity distributions as functions of the angle $\theta$ around the circular cross section of the cone are introduced into these integrals which can be evaluated numerically by the Romberg method. First, the starting point is taken at the upper reattachment point ($\theta = 180°$ if $\alpha$ is large enough) and proceeding clockwise (for the right hand side of the cone) the point where the top boundary layer leaves the surface is identified. Similarly, starting at $\theta = 0°$ and proceeding

**TABLE 2**
**Separation criteria for boundary layer and wall jet**

| Laminar boundary layer | Turbulent boundary layer | Wall jet |
|---|---|---|
| $\left(\frac{\theta_{22}}{\tau_{\eta,0}}\right)\left(\frac{d\rho}{d\eta}\right) \simeq 0{\cdot}7$ | $\left(\frac{\theta_{22}}{\tau_{\eta,0}}\right)\left(\frac{d\rho}{d\eta}\right) \simeq 4{\cdot}7$ | $\left(\frac{\zeta_m}{\tau_{\eta,0}}\right)\left(\frac{d\rho}{d\eta}\right) \simeq 4.$ |
| | Typically<br>$\zeta_m \ll \theta_{22}$<br>And<br>$(\tau_{\eta,0})_{WJ} \gg (\tau_{\eta,0})_{BL}$<br>So<br>$\left(\frac{d\rho}{d\eta}\right)_{WJ} \gg \left(\frac{d\rho}{d\eta}\right)_{BL}$ | |

$\tau_0$: wall shear stress with zero pressure gradient

counterclockwise (for the right-hand side of the cone again) the point where the boundary layer leaves the surface is identified for the two cases of laminar and turbulent boundary layers. For a given cone geometry and angle of attack, the only acceptable solution (in terms of the assumed separation angle) is the one which yields the same pressures at both points where the boundary layer leaves the surface. This implies that the secondary flow is weak. Although an experimental account for the pressure at the separation points has not been found, observations of separated flows on conical bodies have shown that the secondary flow, if it exists, is indeed weak. Thus, the assumption that the pressure is the same at both separation points seems plausible.

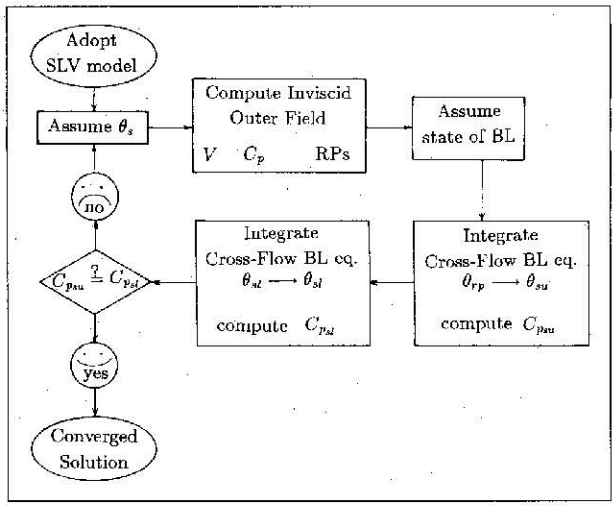


Figure 2. Flow chart for the viscous/inviscid interaction.

Figure 3 shows the converged solutions for a cone with $\varepsilon = 5°$ at $\alpha = 30°$ for laminar and turbulent boundary layers. It may be seen that the main difference between the two cases is the location of the lower separation. As was expected, when the boundary layer is turbulent, separation is delayed until a larger angle. The location of the upper and inviscid separations as well as the vortex positions are almost identical for the two cases.

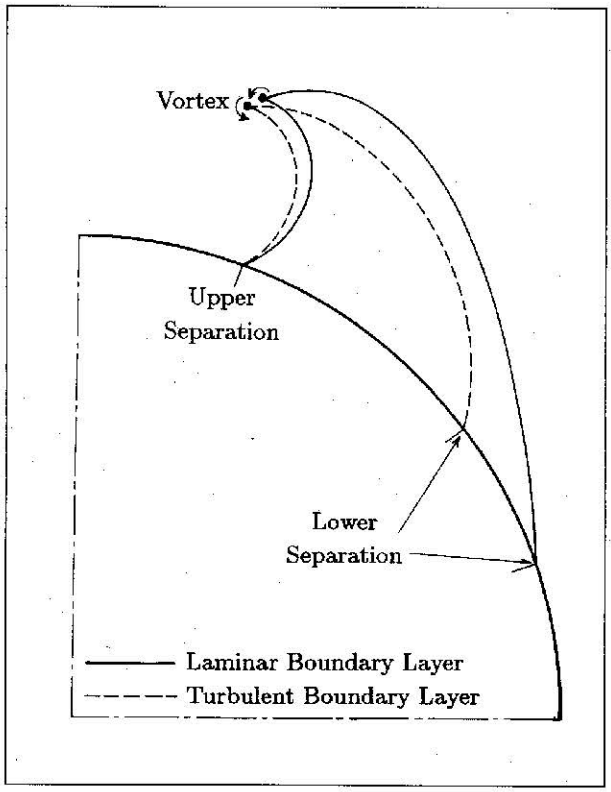


| | Laminar boundary layer | Turbulent boundary layer |
|---|---|---|
| Lower separation | 109° | 127° |
| Vortex sheet location | 147° | 149° |
| Upper separation | 160° | 160° |
| Vortex location | (0·375, 1·285) | (0·349, 1·269) |

Figure 3. Converged solutions for $\varepsilon = 5°$, $\alpha = 30°$.

In Fig. 4 the experimental results of Friberg[6,7] and Jorgensen[8] are shown together with predictions from the present theory. Both sets of experiments involved turbulent boundary layers. The flat part which is common to all the curves in the low range of angles of attack represents attached flow (no vortex solutions exist in this range). At $\alpha \approx 5°$, which corresponds to $\alpha/\varepsilon \approx 1$ in the experiments, separation first takes place and all the separation angles change rapidly as $\alpha$ increases. Finally, at $\alpha \approx 15°$, which corresponds to $\alpha/\varepsilon \approx 3$, each separation angle reaches a limiting value which remains constant as $\alpha$ increases. The agreement

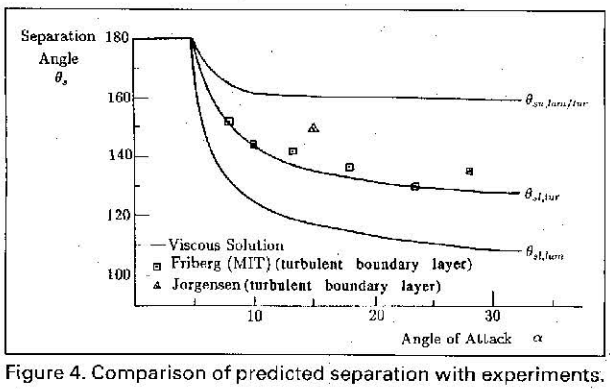


Figure 4. Comparison of predicted separation with experiments.

of the theoretical predictions with experimentally determined points is excellent. Most points fall near the predicted lower separation curve for the case of a turbulent boundary layer.

The modified pressure distribution including the effects of the boundary layer calculation for $\alpha/\varepsilon = 2$ is shown in Fig. 5 for the turbulent boundary layer. The flat portion of the curve represents the separation region where the pressure is required to be uniform.

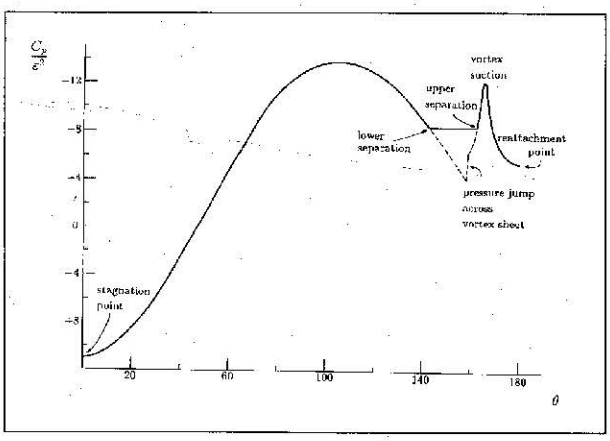


Figure 5. Modified pressured distribution on a circular cone for turbulent boundary layer, $\alpha/\varepsilon = 2$, $\theta_s = 159°$.

## CONTROL OF SEPARATION BY BLOWING

So far it has been shown that the boundary layer on a circular cone at incidence, as it develops from the windward stagnation line towards the leeward generator, will separate due to the adverse pressure gradient. It is possible, however, to postpone this separation, by replacing the natural boundary layer with a turbulent wall jet[1,9]. The increased momentum near the surface reenergises the boundary layer and delays the separation of the viscous flow. The mechanism of delaying the boundary layer separation through blowing is sketched in Fig. 6. This modification of the location of separation requires that all the vortex parameters (position, strength and lift) also be modified to maintain equilibrium. In other words, blowing changes the entire (inviscid) outer flow field by modification of the (viscous) inner flow field.

Although there is an external flow, the jet velocity is assumed to be much higher than the velocity of the outer field. Therefore the jet will be treated as issuing into quiescent surroundings. In addition, since the thickness of the boundary layer and the width of the jet are small compared to the local radius of the cone, curvature effects will also be neglected.

The profile of the wall jet is shown in Fig. 7. The jet consists of two parts; an inner flow adjacent to the wall having a highly non-linear velocity profile characteristic of a turbulent wall flow, and an outer flow having a velocity profile typical of a free turbulent plane jet. The analysis used is that due to Roberts[9].

The only pressure gradient to which the jet is subject, after neglecting curvature effects, is the one due to the external flow. Table 2 compares the separation criteria for the boundary layer and the wall jet. The right side is approximately the same for both cases. The wall jet, however, has greater momentum near the wall. As a result, its characteristic dimension (distance of maximum velocity from the wall) is smaller than the corresponding characteristic dimension of the boundary layer (momentum thickness). In addition,

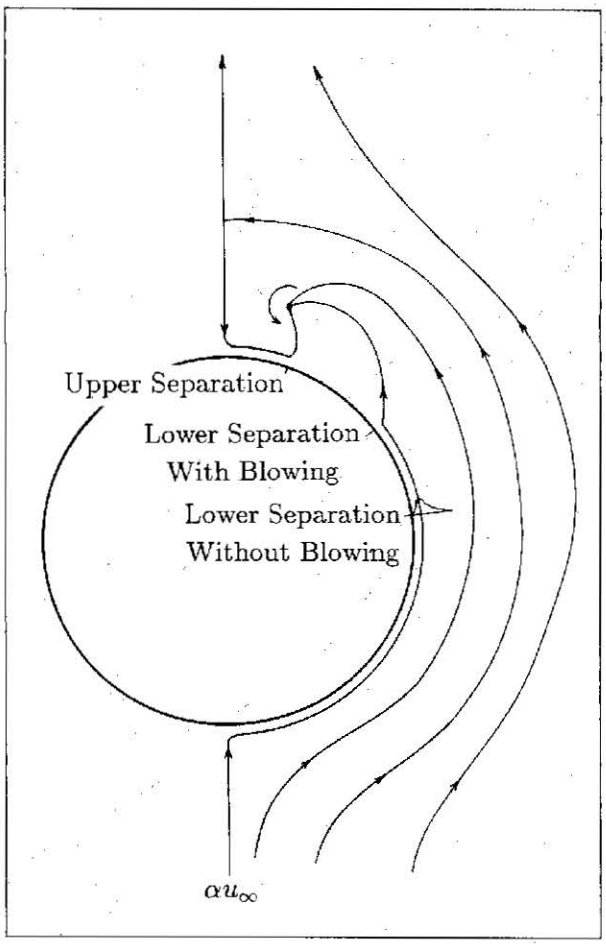


Figure 6. Schematic of controlled boundary layer separation with a wall jet in the cross-plane of a circular cone.

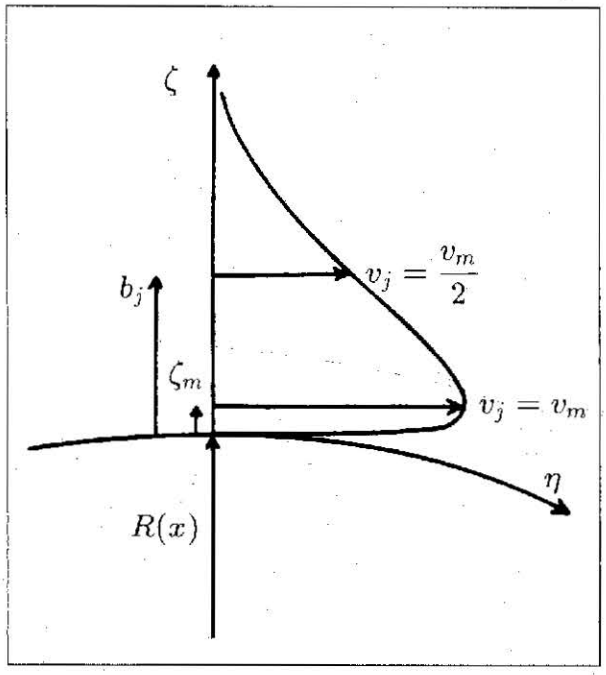


Figure 7. Wall jet profile.

higher velocities near the wall imply larger velocity gradients which result in greater shear stress at the wall. Thus, the first factor on the left side of the separation criterion is much smaller for the wall jet than for the boundary layer. As a consequence, the pressure gradient at separation is much larger for the wall jet and enables it to go farther against an adverse pressure gradient.

The separation condition for the wall jet can be transformed[2] into

$$(\Delta\theta_s)^2 = \frac{21{\cdot}527}{(1+\alpha^2)}\left[\frac{V^2}{\partial C_p/\partial\eta}\right]_s C_\mu \qquad \ldots \quad (9)$$

where $\Delta\theta_s$ is the change in the angular position of the lower separation point due to blowing. The blowing coefficient is defined as the ratio of the jet momentum to that of the external field, just outside the boundary layer

$$C_\mu \equiv \frac{b_j v_m^2}{R v_e^2} \qquad \ldots \quad (10)$$

Equation (9) is plotted in Fig. 8. It is seen, that the blowing intensity required for a given displacement of the lower separation point depends only on the state of the boundary layer (i.e., whether it is laminar or turbulent), and is almost independent of the cone geometry and angle of attack, as is indicated by the almost horizontal curves.

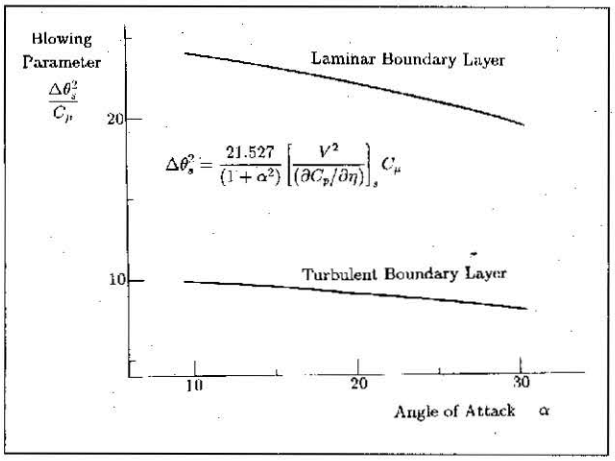


Figure 8. Blowing parameter versus angle of attack.

Figure 9 shows the converged solutions for a cone with $\varepsilon = 5°$ and $\alpha = 30°$ for the case of a turbulent boundary layer before and after blowing. The main observation is that very small blowing intensities are required to move the separation points from their natural locations, as predicted by the viscous/inviscid iteration scheme, to points very close to the leeward generator. The blowing causes the separation to occur at a larger angle from the windward stagnation line, thus moving the vortices closer to the surface of the body toward the leeward generator.

The modified pressure distributions for the configurations shown in Fig. 9, including the effects of the wall jet, are plotted in Fig. 10. It is seen that blowing has the following effects:

It reduces the distance between the upper and lower separation points. This is shown by the diminishing of the flat portion of the curves.

It pushes the vortex (and as a result the vortex suction) closer to the leeward generator, thus closing the flow field. In the limit, as separation is suppressed completely, the results from the Jones theory are recovered.

It weakens the vortices (as is shown from the diminishing vortex suction). This is required to maintain equilibrium of the cross-flow as the vortex approaches the surface. This reduces the vortex lift contribution, which is equivalent to reducing the effective angle of attack. The last observation agrees with experimental results (Ref. 1) and confirms that blowing allows control of the lift on a highly manoeuvrable aircraft without changing its attitude.

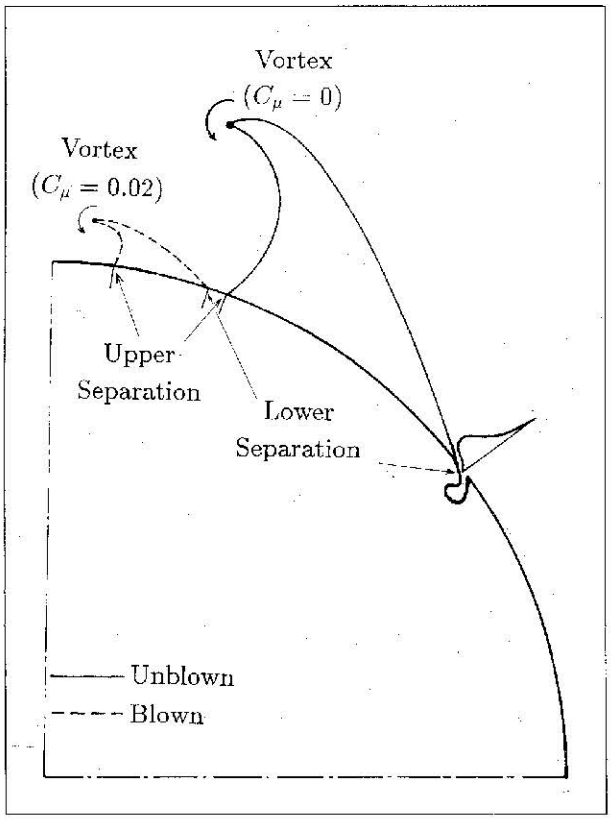


| | Turbulent boundary layer | Turbulent wall jet |
|---|---|---|
| Blowing coefficient | 0 | 0·02 |
| Lower separation | 127° | 162° |
| Vortex sheet location | 149° | 170° |
| Upper separation | 160° | 173° |
| Vortex location | (0·349, 1·269) | (0·090, 1·079) |

Figure 9. Converged solutions before and after blowing ($\varepsilon = 5°$, $\alpha = 30°$, turbulent boundary layer).

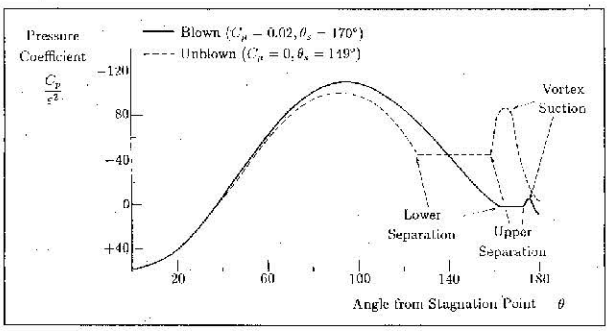


Figure 10. Pressure distribution before and after blowing ($\varepsilon = 5°$, $\alpha = 30°$, turbulent boundary layer).

The relation between the lift and blowing coefficients is shown in Fig. 11. The fact that the curves drop more sharply as the relative incidence ($\alpha/\varepsilon$) increases, indicates that for a given body ($\varepsilon$), blowing becomes more effective as the angle of attack increases. This is also in agreement with experiments[1].

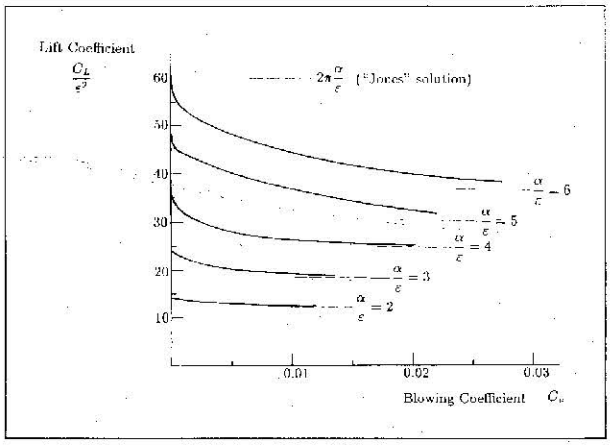


Figure 11. Lift versus blowing.

## DISCUSSION

The present analysis confirmed that blowing is a viable mechanism for controlling the vortex lift on a circular cone and verified trends observed in experiments. The implications of the various assumptions made in this model are discussed below.

The SLV model has the following disadvantages when used to represent the inviscid outer field about bodies at high angle of attack:

The position of the vortices is not very accurate. This should be expected, since the vortices are represented only globally in this model. In reality, the vorticity which is shed from the surface of conical bodies at incidence is distributed and not concentrated as the SLV model assumes. More complicated models which take this fact into account (for example, Ref. 10) give vortex core locations which agree much better with experimental observations. Nevertheless, the crude vortex locations given by the SLV model are very useful as initial guesses for the more complex numerical models.

The vortex lift is overestimated. This again is the result of a very strong suction generated on the upper surface of the body under the locations of the vortices. For most bodies, however, the non-linear lift is not a large part of the total, hence the error in the total lift is not too serious.

Vortex solutions cannot be found below a minimum value of the relative incidence, which depends on the thickness of the body and the location of separation. Experimental observations (Refs. 6-8), partially verify this result, since at small angles of attack the body radius, as it grows in the longitudinal direction, prevents the departure of free vortices. When the angle of attack becomes sufficiently high, the vorticity in the boundary layer accumulates along generators on the upper surface of the body. The vortices generally do not separate from the body until some higher angle of attack is reached.

The pressure distribution is poorly predicted by this theory, principally because the vorticity in the feeding sheets is neglected. On the body surface, the pressure

jumps at the point where the vortex sheet emanates. This is also physically impossible. In reality the vortex sheet adjusts its position and shape so that it coincides with a 3-D stream surface. Since the normal velocity across such a surface is zero, the force on the vortex sheet is zero as well. In this model, however, the pressure jump is necessary to create the force on the vortex sheet which balances the force on the vortex.

The boundary layer solution agrees very well with experiments in terms of the predicted separation points. Although this might have been expected when the terms that dropped out of the cross-flow momentum equation were found to be small, there was still the question of how an unrealistic pressure jump resulting from the SLV model would affect the boundary layer solution. Fortunately, because the lower boundary layer separates well before the point where the vortex sheet emanates (for the inviscid solution), the calculation of the boundary layer takes place in a region which is not affected much by the pressure jump across the vortex sheet.

The use of 2-D separation criteria (despite the fact that the flow is actually 3-D) is justified by the conicality of the flow. Even though the growth of a laminar boundary layer cannot be conical, because the exponent in equation (8), is 0·5, for a turbulent boundary layer the exponent is near unity, implying a flow field very close to conical conditions. This, combined with an external conical flow, results in a flow field which is dominated completely by the circumferential pressure gradient, to the extent that the separation lines are also conical.

The wall jet solution also agrees well with experiments despite the fact that some simplifications were made in the model. The assumption that the jet issues into quiescent surroundings was necessary to get a self-similar solution which in turn allowed the simple relation between $C_L$ and $C_\mu$ shown in Fig. 11. The assumption of negligible curvature, actually underestimates the effects of the blowing which are enhanced when curvature is present (Coanda effect).

In regard to the reduction in the lift due to blowing (Fig. 11) the following discussion applies. At the high angles of attack to which some of the highly manoeuvrable aircraft operate, the main problem is to eliminate any asymmetries of the vortex system, vortex breakdown, or both. Thus, the desire to sacrifice some of the vortex lift in order to achieve this goal is not surprising. On the other hand, blowing does not always reduce the vortex lift. At angle of attack beyond the point of maximum unblown lift[1], blowing actually increases the vortex lift because it stabilises the vortex system which otherwise would have broken down.

An alternative way to stabilise the vortices would be blowing from the apex along the axes of the vortices. However, controlling the conditions which produce the vortices (i.e., boundary layer separation), is a more effective way to achieve our goal. This is indicated by the fact that very little tangential blowing produces very large changes in the vortex system.

Smaller blowing intensity is required for the turbulent boundary layer for the same final configuration. This is explained by the fact that the separation for the turbulent boundary layer occurs naturally at a larger angle, and therefore the required $\Delta\theta_s$, is smaller.

## CONCLUSIONS

(i) Displacement of the vortex separation has been shown to influence the location and strength of the vortices on a circular cone.

(ii) The 3-D boundary layer over a circular cone has been analysed. A metehod analogous to the von Karman/Pohlhausen technique has been used to solve the cross-flow momentum equation, and the predicted separation lines agree well with experiments.

(iii) Blowing tangentially from slots located symmetrically along cone generators near the point of cross-flow separation is an effective way to control vortex location and strength. For sufficiently large blowing the dependence on vortex lift can be drastically reduced, and the effects of flow asymmetries may be made negligible.

## REFERENCES


1. WOOD, N. J. and ROBERTS, L. The control of vortical lift on delta wings by tangential leading edge blowing, *AIAA* paper no. 87-0158, January 1987.
2. MOURTOS, N. J. Control of vortical separation on conical bodies, PhD Thesis, Department of Aeronautics and Astronautics, Standford University. Also: Stanford/NASA Ames Joint Institute for Aeronautics and Acoustics TR-78.
3. BRYSON, A. E. Symmetric vortex separation on circular cylinders and cones, *J Appl Mech*, December 1959.
4. JONES, R. T. Properties of Low Aspect Ratio Pointed Wings at Speeds Below and Above the Speed of Sound, NACA report no. 835, 1946. Also: NACA TN-1032, 1946.
5. SCHLICHTING, H. *Boundary Layer Theory*, McGraw Hill Inc, San Francisco, 1979, p 206.
6. FRIBERG, E. G. Measurement of vortex separation, Part I: Two-dimensional circular and elliptic bodies, MIT TR-114, August 1965.
7. FRIBERG, E. G. Measurement of vortex separation, Part II: Two-dimensional circular and elliptic bodies, MIT TR-115, August 1965.
8. JORGENSEN, L. H. Elliptic Cones alone and with wings at supersonic speeds, NACA TN-4045, October 1957.
9. ROBERTS, L. A theory for turbulent curved wall jets, *AIAA* paper no. 87-0004, January 1987.
10. SMITH, J. H. B. Improved calculations of leading edge separation from slender, thin, delta wings, *Proc R Soc A*, 1968, **306**, pp 67-90.